AGU PUBLICATIONS

JGR

Journal of Geophysical Research: Atmospheres

RESEARCH ARTICLE

10.1002/2016JD026445

On the relative importance of radiative and dynamical heating for tropical tropopause temperatures

Thomas Birner[1] and **Edward J. Charlesworth**[1]

[1] Department of Atmospheric Science, Colorado State University, Fort Collins, Colorado, USA

Key Points:
- Structural sensitivity of tropical tropopause layer temperatures to water vapor and ozone radiative heating
- Transport-radiation feedbacks, particularly strong due to ozone
- Ozone spread alone can explain large fraction of spread in cold point temperatures in climate models

Correspondence to:
T. Birner,
thomas.birner@colostate.edu

Citation:
Birner, T., and E. J. Charlesworth (2017), On the relative importance of radiative and dynamical heating for tropical tropopause temperatures, *J. Geophys. Res. Atmos.*, *122*, 6782–6797, doi:10.1002/2016JD026445.

Received 31 DEC 2016
Accepted 16 JUN 2017
Accepted article online 20 JUN 2017
Published online 4 JUL 2017

Abstract The tropical tropopause layer (TTL) shows a curious stratification structure: temperature continues to decrease beyond the level of main convective outflow (~200 hPa) up to the cold point tropopause (~100 hPa), but the TTL is more stably stratified than the upper troposphere. A cold point tropopause well separated from the level of main convective outflow has previously been shown to be consistent with the detailed radiative balance in the TTL even without dynamical effects. However, the TTL is also controlled by adiabatic cooling due to large-scale upwelling within the Brewer-Dobson circulation, which creates the extremely low stratospheric water vapor content via freeze drying. Here we study the role of water vapor and ozone radiative heating on the detailed temperature structure of the TTL based on idealized single-column radiative-convective equilibrium simulations. An atmosphere without adiabatic cooling due to upwelling results in much higher stratospheric water vapor content; the resulting altered radiative heating structure is shown to push the TTL in a regime of radiative control by water vapor. The TTL structure is furthermore shown to be strongly sensitive to the altitude where ozone sharply transitions from tropospheric to stratospheric values. Adiabatic cooling due to upwelling is found to reduce the radiative control by water vapor, resulting primarily in a negative transport-radiation feedback. Conversely, the radiative control by ozone is enhanced due to upwelling—a positive transport-radiation feedback. The particularly strong ozone radiative effect may explain about half of the reported spread in cold point temperatures (~10 K) in current climate models.

1. Introduction

Air enters the stratosphere predominantly through the tropical tropopause layer (TTL), within the upwelling branch of the Brewer-Dobson circulation. The TTL therefore strongly influences atmospheric tracer amounts entering the stratosphere. For example, the upwelling air is "freeze dried" in the TTL by the extremely cold conditions there [*Brewer*, 1949; *Holton et al.*, 1995]. Hence, the amount of water vapor entering the stratosphere is determined to a large degree by temperatures in the TTL. Stratospheric water vapor plays an important role in the radiative budget of the stratosphere [*Manabe and Strickler*, 1964; *Forster and Shine*, 1999], with potential implications for surface climate [*Solomon et al.*, 2010; *Maycock et al.*, 2013]. The TTL extends broadly from the level of main convective outflow ~200 hPa (~12 km) to the cold point tropopause ~90 hPa (~17 km). It is unique in that it shares both tropospheric and stratospheric characteristics. For example, ozone increases rapidly with height above the level of main convective outflow, whereas temperatures follow tropospheric lapse rates up to the cold point tropopause [*Folkins et al.*, 1999; *Fueglistaler et al.*, 2009].

Temperature variability in the TTL is governed by an unusually large number of processes: dynamics on a vast range of scales, clouds and microphysics, and radiation. Radiative time scales are large in this region, 30–60 days [*Randel et al.*, 2002; *Hitchcock et al.*, 2010]. Seemingly small differences in heating rates, e.g., simulated by climate models, can therefore cause large differences in temperatures. It may then not surprise that current climate models show a wide spread in tropical cold point tropopause temperatures (T_{CP}), of the order of 10 K [*Gettelman et al.*, 2010; *Kim et al.*, 2013; *Randel and Jensen*, 2013]. Water vapor concentrations show a similarly large spread, limiting our current ability to accurately simulate and predict water vapor throughout the stratosphere.

The sensitivity of TTL temperatures to ozone has been pointed out by several studies [e.g., *Manabe and Hunt*, 1968; *Fels et al.*, 1980; *McElroy et al.*, 1992; *Thuburn and Craig*, 2002; *Forster et al.*, 2007]. *Chae and Sherwood* [2007] found that the seasonal cycle in T_{CP} is amplified by the radiative effects of ozone; i.e., the warmer cold point during boreal summer is in part due to the higher ozone levels near the cold point and their associated

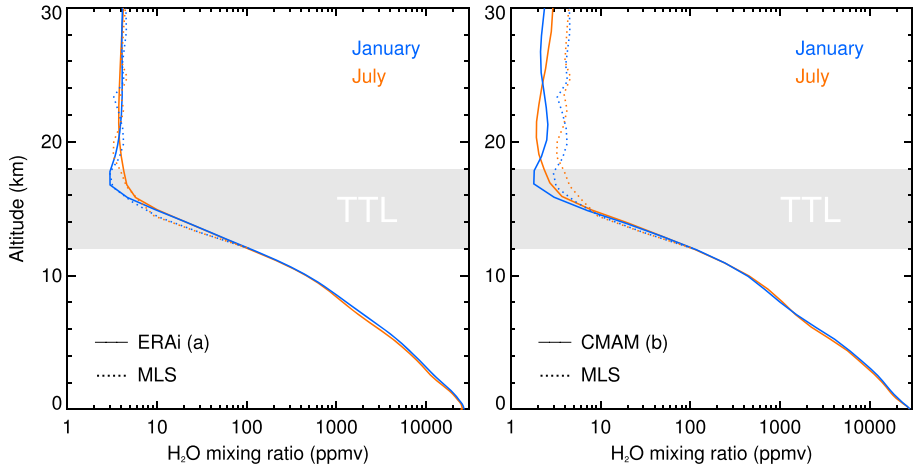

Figure 1. Climatological tropical (5°S–5°N) water vapor profiles, comparing January (blue) versus July (orange) and different data sets (see plot legends). MLS is only valid above ~200 hPa. Shading indicates TTL. Time period used for ERA-I and MLS is 2005–2012.

radiative heating. This effect was confirmed and further studied by *Fueglistaler et al.* [2011], and recently extended to the radiative effects of water vapor by *Gilford and Solomon* [2017] and *Ming et al.* [2017]. *Gettelman et al.* [2009] showed that T_{CP} in chemistry climate models (CCMs) is sensitive to the ozone amount in the TTL, which likely impacts their long-term trends in T_{CP}.

Ozone near the tropical tropopause is strongly shaped by transport and balanced by chemical production and loss [e.g., *Avallone and Prather*, 1996; *Abalos et al.*, 2013]. Convective mixing from below can cause strong reductions in TTL ozone amounts [e.g., *Folkins et al.*, 2002], correlated with tropopause-level cooling [e.g., *Paulik and Birner*, 2012]. Upwelling by the Brewer-Dobson circulation both cools and reduces upper TTL ozone amounts [e.g., *Randel et al.*, 2007a]. Horizontal mixing can cause strong enhancements in tropopause-level ozone amounts, especially during boreal summer and fall [e.g., *Konopka et al.*, 2007]. Feedbacks between transport and radiation due to ozone may be important for TTL temperatures.

Water vapor decays exponentially by about 1 order of magnitude through the TTL (see Figure 1 below) and contributes significantly to radiative heating rates in this region [e.g., *Gettelman et al.*, 2004]. Stratospheric water vapor amounts are predominantly set by the temperature of the cold point tropopause but may feed back onto TTL temperatures, either directly through local longwave cooling or indirectly through downwelling longwave radiation from higher stratospheric levels above [cf. *Manabe and Strickler*, 1964, Figure 9].

Here we study the roles of water vapor and ozone radiative heating on the detailed temperature structure of the TTL, extending the work of *Thuburn and Craig* [2002]. We use a highly idealized modeling approach, based on single-column radiative transfer calculations, incorporating simplified parameterizations of convection and large-scale stratospheric upwelling. Cloud-radiative processes may be important in determining TTL temperatures [e.g., *Yang et al.*, 2010], but our current knowledge of these cloud effects is highly uncertain, which prevents straightforward inclusion of cloud-radiative effects in the TTL in simple single-column models as used here.

We find that TTL temperatures are predominantly shaped by the combined action of adiabatic cooling due to stratospheric upwelling and radiative heating due to water vapor and ozone. The latter tracer profiles are in turn strongly shaped by transport, which leads to transport-radiation feedbacks in the TTL. Stratospheric water vapor is found to primarily cause a negative feedback; e.g., direct cooling due to stronger upwelling is reduced by weaker longwave cooling due to smaller water vapor amount. A stronger positive transport-radiation feedback is found to exist for ozone: direct cooling due to stronger upwelling is amplified by reduced shortwave and longwave heating associated with reduced ozone amount. Comparing scenarios with and without stratospheric upwelling, we find that the water vapor feedback is reduced due to the presence of upwelling, whereas the ozone feedback is enhanced. It should be noted that transport-radiation feedbacks are not studied via fully interactive simulations here but by isolating upwelling-induced adiabatic

cooling and ad hoc changes to the tracer structures. Associated feedbacks due to fully interactive transport and radiation as highlighted in the context of climate change [e.g., *Dietmüller et al.*, 2014; *Nowack et al.*, 2015] are left for future studies.

The paper is structured as follows. Section 2 revisits the basic question raised by *Thuburn and Craig* [2002], whether a TTL-like region may exist in local radiative equilibrium. Section 3 studies the effects of variable stratospheric background amounts of water vapor on TTL temperatures. Section 4 studies the effects of changes to the shape of the ozone profile near the tropopause on TTL temperatures. These two sections do not consider the effects of stratospheric upwelling—these effects are analyzed in section 5. A detailed discussion of our results is provided in section 6.

2. Data and Approach

Our approach centers around single-column radiative transfer calculations. We use the Rapid Radiative Transfer Model (RRTM) [*Mlawer et al.*, 1997], which is a state-of-the-art radiative model based on the correlated-k method (a simplified version, RRTMG, is used in many current climate models). RRTM comes as separate longwave and shortwave components with 16 and 14 spectral bands, respectively. In practice, we run both RRTM components sequentially and time step the temperature equation subject to other constraints (e.g., convective adjustment) as detailed below. We use a time step of 90 min. All experiments are run for 200 days including a diurnal cycle, taking the average over the last 20 days as the equilibrium state. We have found 200 days (roughly 3–4 times typical radiative time scales near the tropical tropopause [*Hitchcock et al.*, 2010]) sufficient to ensure that equilibrium has reached. We will contrast radiative-convective equilibrium (RCE) solutions with the so-called stratospheric radiative equilibrium (SRE) solutions (see below).

Single-column RCE modeling has been widely used since the pioneering works of *Manabe and Strickler* [1964] to understand important features of the vertical structure and heat balance of the atmosphere. In the simplest case, convection is mimicked by adjusting the temperature profile at every time step to a given lapse rate (often 6.5 K/km) wherever the radiatively forced temperature profile tends to exceed this lapse rate. This way, a temperature profile is built with certain assumptions about the dynamics of the tropospheric part of the column and a stratosphere in local radiative equilibrium.

The SRE approach represents an alternative to RCE. It is based on taking a temperature profile with all the effects due to dynamics and radiation incorporated (e.g., from observations or a comprehensive climate model) and then, using an offline radiative transfer model, calculating a hypothetical profile that has its stratospheric part in local radiative equilibrium and its tropospheric part constrained by the initial temperature profile [*Birner*, 2010]. This way, no assumption is needed about dynamical processes setting the tropospheric temperature profile to match a certain lapse rate. That is, the tropospheric lapse rate is allowed to be a function of height with a realistic shape as opposed to a constant. *Birner* [2010] demonstrated the importance of adjusting the tropopause height in these calculations. This SRE solution in its control setting is based on the profiles of radiatively active tracers, most importantly water vapor and ozone, e.g., from observations or a climate model. However, stratospheric distributions of water vapor and ozone heavily depend on transport, which does not exist in SRE. That is, basic SRE solutions still indirectly incorporate dynamical effects (to be discussed in more detail below).

Other details of the setup of the RRTM simulations are as follows. Profiles of water vapor concentrations are either prescribed or interactively calculated as described below. Profiles of ozone concentrations are prescribed as discussed below. Other tracers used by RRTM are prescribed as constant volume mixing ratios (no vertical dependence): carbon dioxide (356 ppmv), methane (1.75 ppmv), carbon monoxide (0.1 ppmv), nitrous oxide (0.32 ppmv), and oxygen (0.21). Vertical grid spacing is given by the underlying data set for the SRE solutions. For the RCE calculations it is set to 200 m up to 32 km altitude with a constant pressure spacing of 0.3 hPa above that altitude and a total of 192 vertical levels. Surface temperature is fixed in all runs, either to that of the underlying data set (SRE) or to 300 K (RCE). Surface emissivity is set to 1 for the longwave and to 0.8 for the shortwave parts of the radiative calculations.

Our SRE simulations discussed in the next section are based on data from the European Centre for Medium-Range Weather Forecasting (ECMWF) Interim reanalyses (ERA-I hereafter) and a free-running comprehensive chemistry-climate model (CMAM—the Canadian Middle Atmosphere Model, same model run as in *Birner* [2010]). Figure 1 shows tropical (5°S–5°N) water vapor profiles from ERA-I and CMAM, each

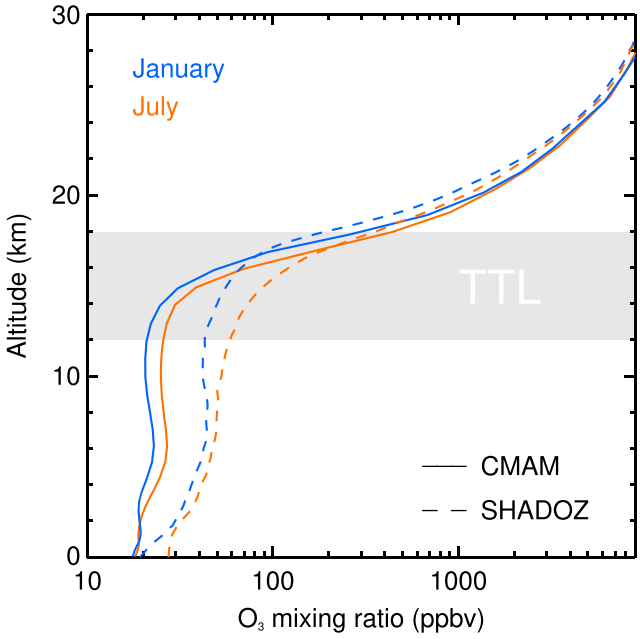

Figure 2. Climatological tropical ozone profiles, comparing January (blue) versus July (orange) and SHADOZ observations (dashed) versus CMAM (full), similar to Figure 2 in *Gettelman and Birner* [2007]. Shading indicates TTL.

compared to observational estimates from the Aura Microwave Limb Sounder (MLS) [*Livesey et al.*, 2007]. The MLS data are only shown for reference but not used for any of the calculations shown below.

Seasonal differences in water vapor are generally small, except near the cold point tropopause. ERA-I shows a fairly large moist bias compared to MLS in the lower half of the TTL, ~40% between 12 and 15 km altitude. Note that ERA-I does not assimilate water vapor data near the tropopause and above; water vapor is primarily constrained by temperatures in this region. Nevertheless, in the lower stratosphere where water vapor is primarily set by tropical tropopause temperatures, ERA-I agrees very well with MLS. In contrast, CMAM agrees with MLS in the lower half of the TTL but shows a dry bias in the upper half and throughout the stratosphere, in part due to a cold bias at the tropical tropopause.

Figure 2 shows tropical ozone profiles from CMAM compared to climatological profiles from the Southern Hemisphere Additional Ozonesondes (SHADOZ) [*Thompson et al.*, 2003] data set for January and July (same as used in *Gettelman and Birner* [2007]). ERA-I ozone is not shown as it is not used in their radiative transfer calculations [*Dee et al.*, 2011]. In the calculations presented below, SHADOZ ozone profiles have been used for results based on ERA-I.

CMAM shows a low bias in tropospheric ozone, which is due to missing tropospheric chemistry in this particular version of the model (see *Gettelman and Birner* [2007] for more details). In the stratosphere, CMAM's ozone is biased high compared to SHADOZ and the sharp transition in the TTL appears to be located too low. There is a significant seasonal cycle evident in the TTL in both data sets.

3. TTL in Local Radiative Equilibrium?

The question may be asked why a TTL exists in the first place and how its temperature structure is formed and maintained. Here and in the following we refer to a TTL broadly as the layer between either the top of the convectively adjusted region (RCE) or the bottom of the radiatively adjusted region (SRE) and the cold point tropopause. *Thuburn and Craig* [2002]—hereafter TC02—found a TTL to exist in local radiative equilibrium in their single-column RCE model. This may be considered to be a remarkable finding because it states that despite the well-known importance of dynamical processes in modulating TTL temperatures in the real atmosphere [e.g., *Manabe and Hunt*, 1968], a TTL-like region can still exist without these dynamical processes. TC02 attribute the existence of this TTL-like region mainly to localized heating due to CO_2 near the convection top. An inclusion of adiabatic cooling, e.g., due to the upwelling branch of the Brewer-Dobson circulation, modified the separation between the convection top and the cold point tropopause. However, TC02 found the TTL-like region to exist even without the cooling effect of the upwelling.

To test whether this finding also holds when using the SRE approach, we have obtained SRE solutions for January and July based on tropical temperature profiles from ERA-I and CMAM (Figure 3). Water vapor and ozone profiles are prescribed based on the underlying data set's climatologies as shown in Figures 1 and 2, where SHADOZ ozone is used for ERA-I. Note that the tropopause level, above which radiative heating rates are applied, is updated at every time step, allowing the tropopause to adjust to the applied radiative heating

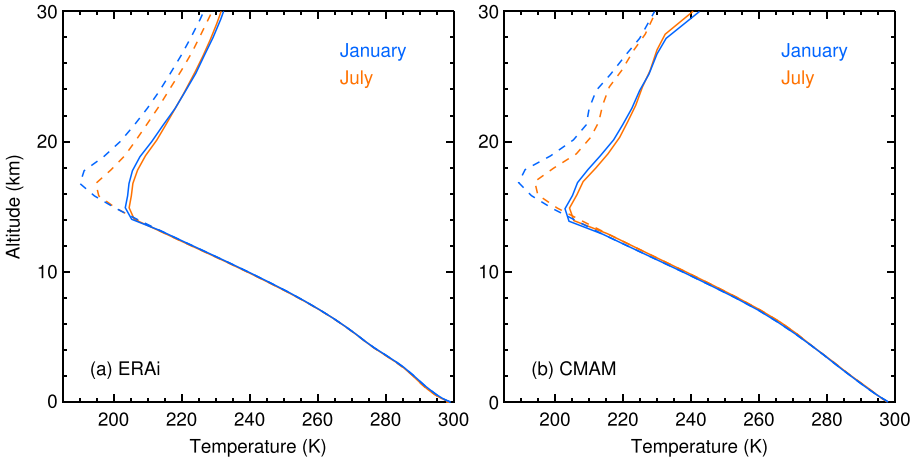

Figure 3. Tropical (5°S–5°N) temperature profiles from (a) ERA-I and (b) CMAM. Full lines represent SRE solutions (see text for details), while dashed lines show respective climatologies from the underlying data.

rates. We use the same (thermal) tropopause definition as in *Birner* [2010], i.e., based on the level of maximum vertical curvature of the lapse rate profile.

By definition, the tropospheric part of these SRE solutions remains unchanged from the underlying data (ERA-I or CMAM). As expected, the stratosphere in the SRE solution (above ~14 km) is considerably warmer due to the missing adiabatic cooling from the upwelling branch of the Brewer-Dobson circulation. More importantly, the TTL shrinks severely in both seasons with the cold point tropopause very close to the convection top (~12 km) [cf. *Gettelman and Birner*, 2007] in the SRE solution. This suggests that in contrast to the TC02 results, a TTL of realistic vertical extent crucially depends on upwelling-induced adiabatic cooling due to the Brewer-Dobson circulation [cf. *Manabe and Hunt*, 1968; *Highwood and Hoskins*, 1998].

Seasonal differences are very small in the SRE solutions (cf. blue versus orange full lines in Figure 3), whereas the stratosphere is colder during January in the underlying ERA-I and CMAM data (cf. dashed lines in Figure 3). A small seasonal temperature difference remains in the SRE solutions. This is due to the seasonal cycle in ozone concentrations in the TTL and lowermost stratosphere; a test using the same ozone profiles for both seasons resulted in almost identical stratospheric temperature profiles (not shown). Note that the radiative feedback due to the ozone seasonal cycle is strongest in spring and fall; i.e., our comparison between January and July only partially demonstrates this feedback. The radiative feedback due to the water vapor seasonal cycle likewise maximizes during spring and fall, with essentially no effect during January and July [*Gilford and Solomon*, 2017; *Ming et al.*, 2017]. The seasonal cycles in water vapor and ozone are in large parts produced by the seasonal cycle in upwelling [*Mote et al.*, 1996; *Randel et al.*, 2007b], as well as horizontal [*Konopka et al.*, 2007; *Ploeger et al.*, 2012] and vertical [*Glanville and Birner*, 2017] mixing; in that sense even the remaining seasonal temperature difference in SRE is of dynamical origin, albeit indirectly. Ozone therefore causes a positive feedback in that stronger upwelling produces stronger adiabatic cooling but also reduced ozone concentrations, which in turn cause reduced radiative heating, hence amplifying the initial response (to be discussed further below).

Figure 3 also shows that stratospheric temperatures in SRE are considerably colder based on ERA-I compared to CMAM (e.g., roughly 224 K in ERA-I versus 228 K in CMAM at 25 km altitude). This must in large parts be due to differences in the water vapor and ozone profiles used in the different calculations. Figures 1 and 2 indicate that the stratosphere in CMAM is biased low in water vapor but high in ozone concentrations. Stratospheric water vapor provides longwave radiative cooling, whereas ozone provides shortwave and longwave radiative heating. Both water vapor and ozone biases therefore contribute to a warmer stratosphere in CMAM's SRE solution.

The question arises why the two approaches—RCE (TC02) versus SRE (see above)—yield fundamentally different answers on whether a TTL-like region of realistic vertical extent can exist in local radiative equilibrium. Both assume a similar fixed surface temperature but a different tropospheric lapse rate structure. Prescribed ozone profiles are similarly based on observations (or a climate model) in both approaches. However, as will

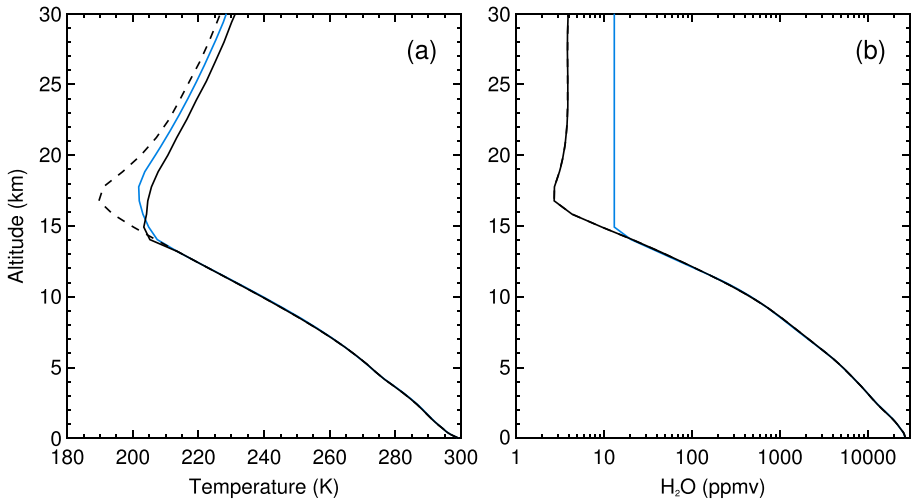

Figure 4. SRE solutions based on tropical (5°S–5°N) ERA-I profiles. (a) Temperature profiles for January ERA-I climatology (dashed), SRE solution with unadjusted water vapor profile (black, full, same as blue full line in Figure 3a), and SRE solution with water vapor adjusted by tropopause temperature (blue). (b) Water vapor profiles as applied for the SRE solutions for January ERA-I climatology at the equator (black) and adjusted by tropopause temperature using 50% relative humidity corresponding to the simulated cold point temperature as in TC02 (blue). See text for details.

be shown below, assumptions about the water vapor distribution produce striking differences in the TTL and stratosphere. The TC02 approach assumes a constant relative humidity and computes the resulting water vapor profile with the constraint that the water vapor mixing ratio cannot increase with height. This way, the simulated stratospheric water vapor amount essentially becomes a function of the model cold point temperature. Since the cold point in RCE is much warmer than in the real atmosphere (by at least 10 K; see Figure 3), the stratospheric water vapor concentration in the RCE/TC02 approach is much larger than in the real atmosphere. The SRE approach on the other hand uses a prescribed water vapor profile where the stratospheric water vapor amount is set by the real atmosphere's cold point temperature, not by that of the SRE solution.

To test whether the difference in stratospheric water vapor concentrations between the two approaches explains their qualitatively different TTL temperature structures, we have repeated the SRE calculation by adjusting the water vapor profile so that it is held constant above a concentration corresponding to 50% relative humidity at the SRE cold point (Figure 4). This produces adjusted SRE stratospheric water vapor concentrations that are a factor of 3–4 larger than in the real atmosphere (blue line in Figure 4b). All other parameters and settings are the exact same as before. Evidently, the stratospheric water vapor concentration has a profound effect on the TTL temperature structure: the extra water vapor produces local longwave cooling and leads to lower temperatures everywhere above ~15 km. This cooling produces a cold point that is well separated from the convection top (by ~3 km).

Both approaches (RCE and SRE) use the observed ozone profile. As discussed earlier, ozone in the TTL is heavily shaped by transport—a lower tropopause in the SRE solution compared to the real atmosphere would be expected to also result in a transition from low tropospheric ozone amounts to high stratospheric ozone amounts to occur at much lower altitudes. The resulting higher ozone amounts just above the SRE tropopause (~14–16 km altitude) would in turn be expected to lead to warming at these levels [cf. *McElroy et al.*, 1992, Figure 18], sharpening the SRE tropopause. This particular transport-radiation feedback was neglected in the SRE solutions presented so far and is roughly estimated in the following.

In Figure 5 our control SRE solution (black full line in Figure 4) is compared to a modified SRE solution in which the ozone profile was adjusted in an ad hoc way by aligning the lowermost stratospheric increase with the simulated tropopause, while leaving the tropospheric (up to the diagnosed, time-dependent tropopause) and middle-to-upper stratospheric (above 25 km) ozone profile unchanged (red line in Figure 5b). This particular adjustment is somewhat arbitrary but is mainly intended to qualitatively test the sensitivity of the SRE solution to the shape of the ozone profile. In particular, the top of the adjusted region is arbitrary, but we have found the results to be not very sensitive to this choice. Note that our adjustment results in larger column ozone amount, which would be expected in the tropics for a stratosphere without transport.

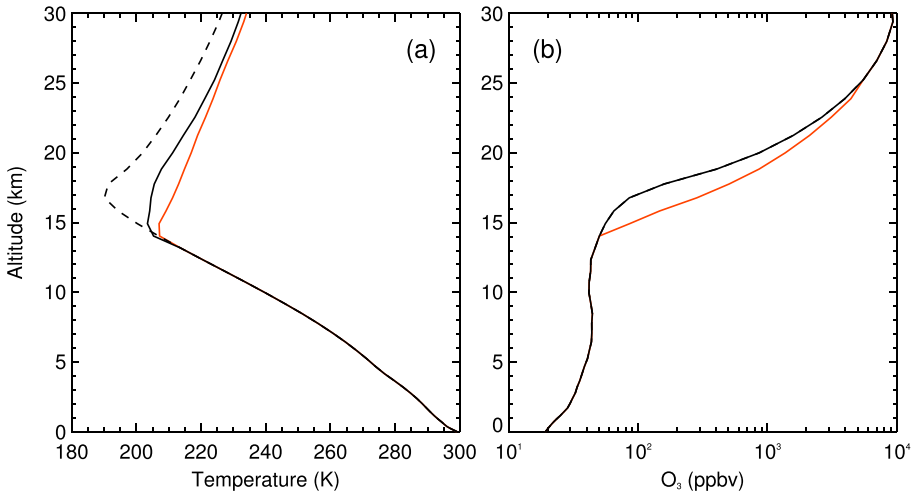

Figure 5. SRE solutions based on ERA-I profiles similar to Figure 4. (a) Temperature profiles for January ERA-I climatology at the Equator (dashed), SRE solution with unadjusted ozone profile (black, full, same as the blue full line in Figure 3a), and SRE solution with adjusted ozone profile (red). (b) Ozone profiles for January SHADOZ climatology (black, same as blue dashed line in Figure 2) and adjusted by tropopause height (red). See text for details.

As expected, the resulting SRE solution is considerably warmer than the control SRE solution in the lowermost stratosphere. The tropopause is sharper, and the cold point coincides with the SRE tropopause, essentially eliminating the TTL.

4. Radiative-Convective Equilibrium With Variable Stratospheric Water Vapor Amounts

In this section the sensitivity of TTL temperatures to background stratospheric water vapor concentrations is explored further. RCE simulations have been performed using the setup of TC02; i.e., surface temperature is fixed at 300 K, convective adjustment is done to a fixed lapse rate of 6.5 K/km, and tropospheric relative humidity is fixed at 50 %. These settings result in near-observed values of temperature and water vapor mixing ratio near the convection top (~14 km). The observed ozone profile based on the SHADOZ stations (dashed blue line in Figure 2) is used as before. For all RCE solutions presented in this paper we set the latitude to 10°S and day of year to 15 January. Note that TC02 used July 15 at 10°N; our setting is almost identical in terms

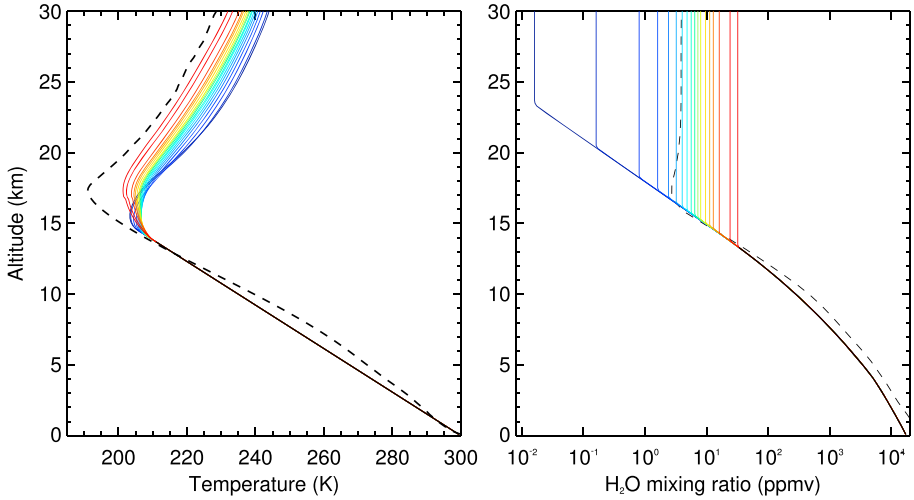

Figure 6. (left) RCE temperature profiles as in TC02 (see text for details) but with (right) variable prescribed minimum water vapor concentrations. Calculations have been performed for January at 10°S. The dashed lines show for reference: a tropical mean radiosonde climatology (obtained from the SHADOZ data set) (Figure 6, left) and the tropical climatological water vapor profile from ERA-I (same as black line in Figure 4) (Figure 6, right).

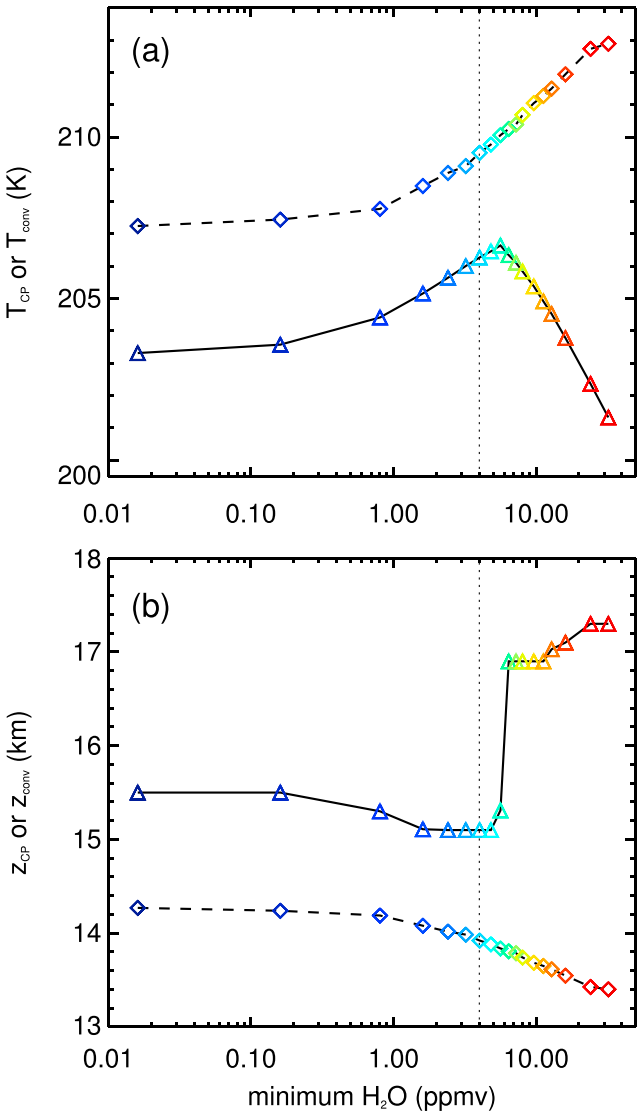

Figure 7. Cold point (triangles, full lines) and convection top (diamonds, dashed lines) (a) temperatures and (b) altitudes as a function of prescribed minimum water vapor amount (q_{str}), corresponding to the temperature profiles shown in Figure 6 (using the same color code). Vertical dotted lines mark approximate observed stratospheric water vapor amount.

of solar zenith angles but uses a latitude more representative of the SHADOZ climatology. Note that this is a slightly different latitude setting from the previous section on SRE solutions.

The main difference to TC02 is that we prescribe a minimum (background stratospheric) water vapor concentration (q_{str}) as follows. At every time step a water vapor profile is first computed based on the prescribed relative humidity of 50%. Then, the altitude where the resulting mixing ratio first falls below q_{str} is obtained and the mixing ratio is set to this value at all higher altitudes. We obtain RCE solutions for a wide range of q_{str} values (3 orders of magnitude, between 10^{-2} ppmv and 10 ppmv). These RCE solutions are shown in Figure 6 (left) with their corresponding water vapor profiles in Figure 6 (right).

Below about 14 km altitude all solutions are equally constrained by their surface temperature and tropospheric lapse rate (black portion in temperature profiles). Above 14 km, however, profiles vary considerably depending on q_{str}. Above about 20 km solutions with higher values of q_{str} are colder due to enhanced longwave cooling, as expected, with temperatures spreading over 10–15 K for the 3 orders of magnitude change in q_{str}. A threefold to fourfold increase in q_{str} over the observed value of ~4 ppmv (cf. Figure 4) leads to enough stratospheric cooling to fully counteract the warming due to missing upwelling-induced cooling in these simple RCE solutions.

Figure 7a shows that the cold point temperature (T_{CP}) depends nonmonotonically on q_{str}: for values of $q_{str} \lesssim 6$ ppmv T_{CP} gradually increases with increasing q_{str}, whereas for $q_{str} \gtrsim 6$ ppmv it strongly decreases with increasing q_{str}. Inspection of Figure 6 reveals that the crossover near 6 ppmv coincides with the layer of constant minimum mixing ratio q_{str} reaching the simulated cold point. That is, for $q_{str} \lesssim 6$ ppmv mixing ratios remain unchanged near the tropopause and the temperature response there depends on the remote stratospheric radiative effects (stronger longwave downward fluxes from the stratosphere for larger q_{str}). On the other hand, for $q_{str} \gtrsim 6$ ppmv mixing ratios are strongly altered at and below the cold point, providing strong local radiative cooling at the cold point. The height of the cold point z_{CP} is roughly constant near 15.5 km for $q_{str} \lesssim 6$ ppmv, whereas for $q_{str} \gtrsim 6$ ppmv a higher cold point above 17 km is formed.

The top of the convectively adjusted region (z_{conv}) lowers somewhat with increasing q_{str}, with the strongest sensitivity in the ~1–10 ppmv range (Figure 7b). This lowering of the convection top is associated with an

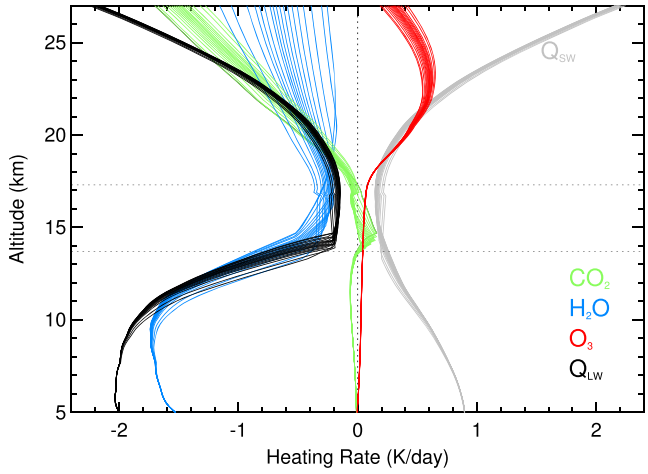

Figure 8. Heating rate sensitivity to changes in q_{str}

increase in its temperature (T_{conv}; see Figure 7a). The separation between the convection top and the cold point (i.e., the notional TTL thickness) is small (~1 km) for $q_{str} \lesssim 6$ ppmv, with a large jump to values above ~3 km for $q_{str} \gtrsim 6$ ppmv. A distinct TTL of several kilometers thickness appears for q_{str} values near or above the observed value.

Figure 8 shows that both the CO_2 and H_2O longwave heating rate (Q_{LW}) structures in the TTL are responsible for shaping its temperature structure. Longwave cooling due to water vapor strongly decreases with height through the TTL, which represents a positive forcing on static stability and helps to separate the convection top from the cold point. The narrow longwave heating due to carbon dioxide near the convection top, on the other hand, produces a negative forcing on static stability in the TTL and helps to maintain the positive lapse rates there (as pointed out by *Thuburn and Craig* [2002]). These two opposing static stability forcings roughly cancel within the TTL (see black lines in Figure 8, showing that the total longwave heating rate is rather uniform with height in the TTL). Note that above the convection top the total radiative heating rate is essentially zero, as demanded by the RCE condition. That is, the net longwave cooling there is balanced by net shortwave heating. Longwave heating due to ozone is small in the TTL, but this is in part due to the fact that the ozone concentrations here are based on the observed TTL (low ozone between 14 and 16 km; see Figure 2) and do not respond to the TTL changes (and implied transport changes) in the RCE runs.

Changes in q_{str} result in changes of Q_{LW} due to all three species (Figure 8). In the background stratosphere (above ~20 km altitude) these individual changes largely compensate each other, even though only the water vapor concentration changes. This shows that the individual longwave contributions are a strong function of temperature. Note that in these RCE runs Q_{LW} may be considered to be effectively constrained by the shortwave heating rate (Q_{SW}) in the region of local radiative equilibrium (i.e., above the convection top). Q_{SW} is essentially given by the ozone profile in the background stratosphere, which remains unchanged here. The inability of Q_{SW} to react to changes in q_{str} and the local radiative equilibrium condition $Q_{LW} + Q_{SW} = 0$ then demand that Q_{LW} should not change much in the background stratosphere. In fact, the only significant changes of Q_{LW} for changes in q_{str} appear near the convection top, because of the sensitivity of z_{conv} to q_{str} and the fact that longwave cooling (primarily due to H_2O) dominates shortwave warming in the convective layer (where $Q_{LW} + Q_{SW} < 0$).

5. Radiative-Convective Equilibrium With Variable Ozone Tropopause Transition Heights

In this section, we explore the sensitivity of RCE temperature profiles to changes in the ozone profile, in particular to the vertical placement of the ozone tropopause transition height z_{O3}. By z_{O3} we refer to the top of the convectively determined tropospheric background of low ozone concentrations—in the real atmosphere $z_{O3} \approx 12.5$ km (Figure 2) and we will refer to this as our reference case. We create a range of ozone profiles in an ad hoc fashion by (1) prescribing a tropospheric background concentration of 43.4 ppbv (the value of the SHADOZ reference profile at 12.5 km altitude), (2) stretching or shrinking the reference SHADOZ profile between [12.5 km, 25 km] altitude and [z_{O3}, 25 km] altitude. Holding the tropospheric background concentration uniform simplifies the treatment of the transition at (the now variable) z_{O3}.

The rationale for these ozone profile modifications is that in the real atmosphere the shape of the ozone profile in and just above the TTL is strongly shaped by transport (primarily due to large-scale upwelling and horizontal mixing and to some extend vertical mixing of low ozone amounts from below). Our RCE

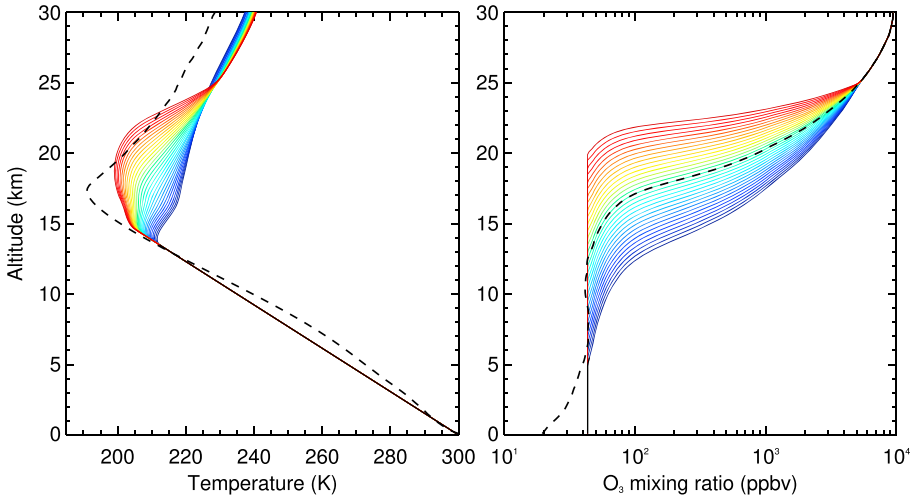

Figure 9. (left) RCE temperature profiles as in TC02 (see text for details) but with (right) prescribed ozone profiles adjusted by variable ozone tropopause-transition heights. Calculations have been performed for January at 10°S. The dashed lines show tropical mean ozonesonde climatologies of temperature (Figure 9, left) and ozone (Figure 9, right) for comparison (obtained from the SHADOZ data set).

simulations assume zero transport above the convection top, which is not reflected in the shape of the prescribed ozone profile. Without transport, ozone mixing ratios in the TTL and lowermost stratosphere would be determined by photochemistry [e.g., *McElroy et al.*, 1992]. By varying the ozone tropopause transition height, we essentially mimic the effects of different transport strengths on the ozone profile near and just above the TTL.

The resulting ozone profiles and corresponding RCE temperature profiles based on our ad hoc modification are shown in Figure 9. The minimum water vapor concentration (q_{str}) is set to 4 ppmv (dotted line in Figure 7), and all other settings in these calculations are identical to those presented earlier.

Our ozone profile modifications via varying z_{O3} result in significant ozone concentration changes of up to 1 order of magnitude in the TTL region (Figure 9, right). These ozone changes lead to large RCE temperature changes between the convection top and the lowermost stratosphere (Figure 9, left). The RCE solution with $z_{O3} = 5$ km (dark blue) is more than 20 K warmer at 19 km altitude than the RCE solution with $z_{O3} = 20$ km (dark red), due to much stronger radiative heating inside the layers affected by ozone increase induced by lowering z_{O3}. The ozone changes furthermore lead to significant structural changes in TTL temperatures: for low z_{O3} a sharp cold point results that is located near the convection top, while for high z_{O3} a broad TTL region results with the cold point well separated from the convection top. These results are broadly consistent with *McElroy et al.* [1992, Figures 17 and 18].

The convection top and cold point characteristics as a function of z_{O3} are further quantified in Figure 10. Higher ozone transition values result in smaller ozone concentrations in the TTL, so both the convection top and the cold point tend to cool and shift to higher altitudes for higher z_{O3}. However, at the highest z_{O3} this effect tends to saturate for the convection top (diamonds), whereas it amplifies for the cold point (triangles). A jump in z_{CP} happens just above the reference $z_{O3} = 12.5$ km. For $z_{O3} \geq 14$ km ozone concentrations remain low throughout the TTL (cf. Figure 9), which may cause this crossover behavior.

6. Effects of Stratospheric Upwelling

In the real atmosphere adiabatic cooling within the upwelling branch of the Brewer-Dobson circulation represents a leading order contribution to the TTL heat budget:

$$Q_{\mathrm{dyn}} \equiv -\overline{w}^{*}(\partial_z T + g/c_p)\,,$$

where $\overline{w}^{*}$ is the residual mean vertical velocity, g is the acceleration due to gravity, and c_p is the heat capacity of air at constant pressure. In this section the effect of stratospheric upwelling on TTL temperatures is studied by prescribing an upwelling velocity. Note that prescribing $\overline{w}^{*}$ does not by itself prescribe the dynamical

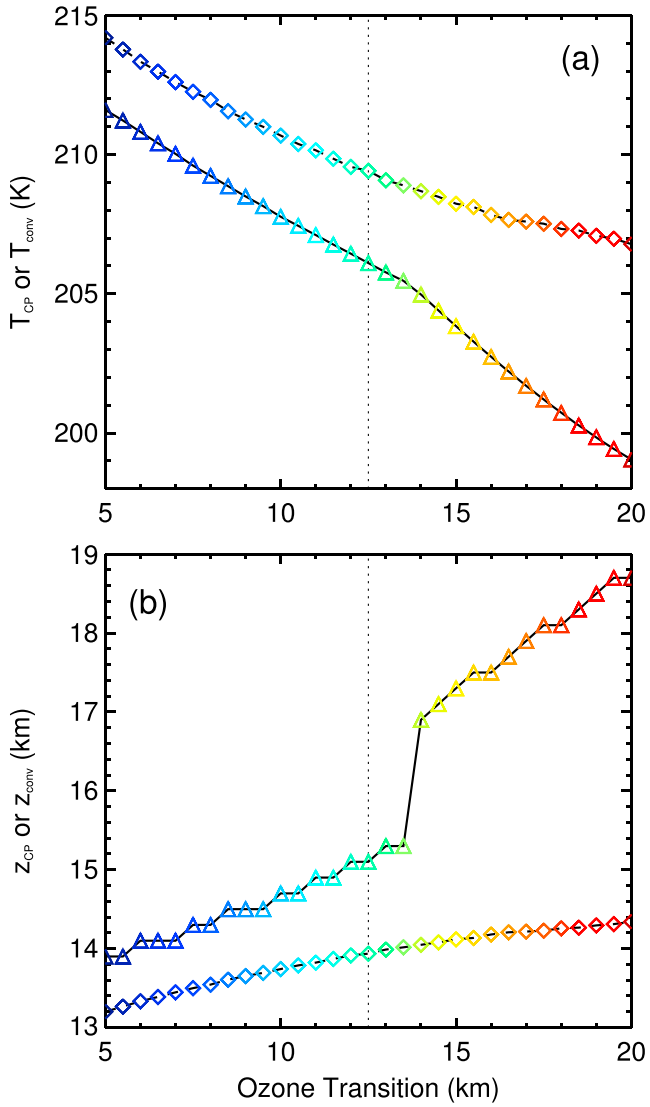

Figure 10. Cold point (triangles, full lines) and convection top (diamonds, dashed lines) (a) temperatures and (b) altitudes as a function of prescribed ozone tropopause-transition height, corresponding to the temperature profiles shown in Figure 9 (using the same color code). Vertical dotted lines mark approximate observed ozone transition height.

cooling, Q_{dyn}, which is also a function of the stratification. In particular, if the temperature profile approached a dry adiabat, given by $\partial_z T = -g/c_p$, the dynamical cooling would vanish. The cooling effect of a given upwelling velocity is therefore in principle limited by the proximity of the temperature profile to a dry adiabat. If, instead, Q_{dyn} was prescribed, then a nearly dry adiabatic temperature profile would demand unphysically large upwelling velocities. Obviously, by setting the tropospheric lapse rate to something less than a dry adiabat (as is done here via the convective adjustment), this unphysical behavior is limited. Nevertheless, it seems more physical to prescribe the mechanically forced upwelling velocity of the stratospheric circulation. Modifications of the radiative tracer distributions due to the transport associated with the imposed upwelling and the associated feedbacks on the temperature structure in and above the TTL are left for future work and not taken into account here. That is, transport-radiation feedbacks are not studied via fully interactive simulations but by isolating upwelling-induced adiabatic cooling and ad hoc changes to the tracer structures (as in the previous sections).

We set $\overline{w}^* = 0.5$ mm/s (close to the real-atmospheric upwelling velocity near the tropopause [e.g., *Abalos et al.*, 2015]) and test how this modifies the sensitivity of the simulated TTL temperatures to changes in minimum water vapor amount q_{str} and ozone tropopause-transition height z_{O3} (Figure 11). In initial experiments with vertically uniform upwelling extending from the surface to the top of the domain we found an unrealistically strong sensitivity of the convection top to the imposed upwelling, which we interpret to be primarily due to the simplistic representation of convection via the lapse rate adjustment. To minimize this sensitivity of the convection top, we only apply the upwelling at and above the first level above the convection top.

As suggested by the temperature difference between the SRE solutions and reference profiles in Figure 3, stratospheric upwelling generally induces cold points that are ~15–20 K colder compared to a stratosphere in radiative equilibrium and this is confirmed by running our RCE simulations with prescribed upwelling as described above (Figure 11). However, cold point temperatures for different TTL ozone or water vapor distributions are not simply offset by a given amount of dynamical cooling. The imposed upwelling has a strong effect on how changes to the radiative tracer distributions might impact the TTL temperature structure. The cold point height is not very sensitive to changes in q_{str} with imposed upwelling (compared to the case without upwelling; cf. Figure 7). With imposed upwelling the cold point temperature is found to be much more

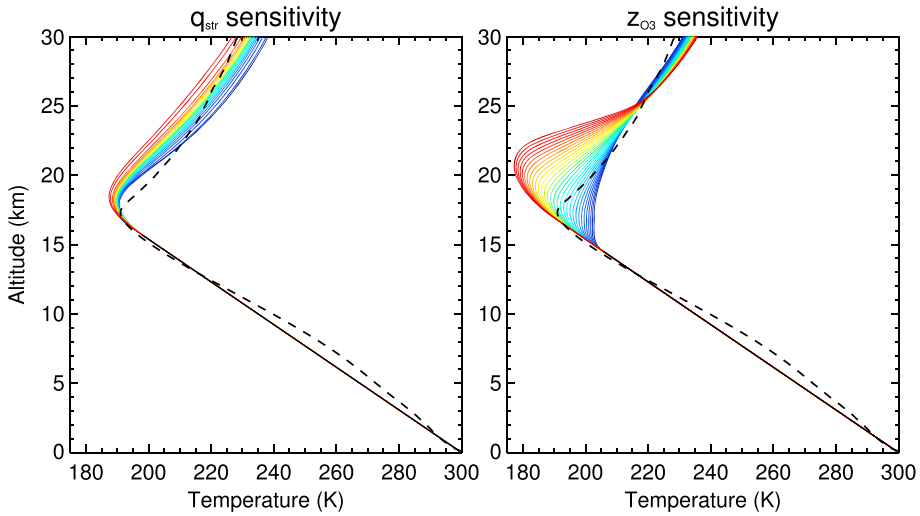

Figure 11. RCE temperature profiles showing sensitivity to (left) prescribed q_{str} and (right) prescribed z_{O3}, similar to Figures 6 (left) and 9 (left) but for imposed stratospheric upwelling of 0.5 mm/s (see text for details). The colors correspond to the water vapor profiles in Figure 6 (right) (dark blue refers to lowest q_{str}) (Figure , left) and the ozone profiles in Figure 9 (right) (dark blue refers to lowest z_{O3}) (Figure , right). The dashed lines show tropical mean temperature climatologies for reference (obtained from the SHADOZ data set).

sensitive to changes in z_{O3}, compared to the case without upwelling (further quantified below). Near its reference value of $z_{O3} = 12.5$ km, the cold point cools by ≈0.7 K km change in z_{O3} when no upwelling is imposed (cf. Figure 10a); this sensitivity amplifies by about a factor of 3 with the imposed upwelling. We conclude that in the real atmosphere, where upwelling near the tropopause is roughly as strong as imposed here, TTL temperatures are particularly sensitive to changes in the ozone profile.

7. Discussion

The sensitivity of stratospheric temperatures to different prescribed stratospheric water vapor concentrations was already studied by *Manabe and Strickler* [1964], but their experiments had too coarse vertical resolution (four layers between 10 and 20 km) to resolve the detailed structure of the tropopause region, and they did not study the sensitivity of tropopause temperatures. Here we find large structural changes in TTL temperatures for variations in background stratospheric water vapor. Our experiments used changes in q_{str} over 3 orders of magnitude, a range that is much larger than any variations of q_{str} occurring in the real atmosphere (e.g., due to seasonal, interannual, or longer-term changes). Nevertheless, the largest sensitivity of TTL temperatures in RCE occurs as the temperature profile goes through a quasi-isothermal state and this happens near the observed value of $q_{str} \approx 4$ ppmv. Largest sensitivity is expected for quasi-isothermal temperature structure, as the cold point becomes ill-defined and can jump several kilometers for small parameter changes.

While longwave cooling to space is the primary radiative effect of stratospheric water vapor in the stratosphere, the TTL also receives downward longwave radiation from the stratosphere. This leads to warmer TTL temperatures for large q_{str} compared to vanishingly small q_{str} (at least as long as q_{str} is not too large; cf. Figure 6). It is interesting then that the reduced q_{str} due to upwelling amplifies the upwelling-induced adiabatic cooling in the TTL via reduced downwelling longwave radiation from the stratosphere—a positive feedback.

The stratospheric water vapor content is to first order set by the cold point temperature T_{CP} via freeze drying; i.e., smaller T_{CP} leads to smaller q_{str} and vice versa. The relationship between T_{CP} and q_{str} in RCE (see Figure 7) then suggests that any initial change to T_{CP} (e.g., due to changes in surface temperature with climate change) will either be amplified (a positive feedback) or reduced (negative feedback) due to the radiative impact from the resulting change in q_{str}. Figure 12(left) shows that the crossover between positive and negative feedbacks occurs roughly at $q_{str} \sim 5$ ppmv in our RCE solutions without imposed upwelling (transition from positive to negative values in the figure). However, with imposed upwelling this feedback is muted due to dynamical cooling near the cold point and for real-atmospheric values of q_{str} it becomes primarily negative

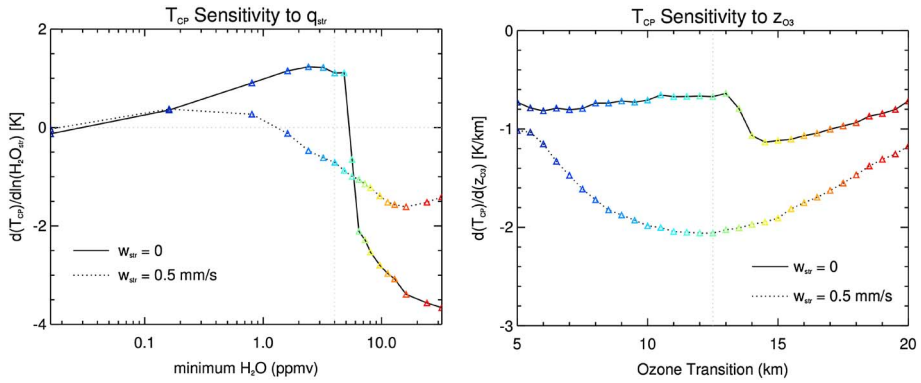

Figure 12. Change in cold point temperature T_{CP} per logarithmic change in (left) prescribed minimum water vapor amount q_{str} (in K) and (right) per change in prescribed ozone tropopause-transition height z_{O3} (K/km). Full lines represent RCE solutions without stratospheric upwelling (control), and dotted lines represent solutions for constant stratospheric upwelling of 0.5 mm/s. Vertical dotted lines mark approximate observed reference values.

(dotted line in Figure 12, left). The effect of the upwelling can be interpreted as lofting the cold point out of the region of exponential decrease of water vapor, into a region where its radiative impact on temperature structure is less strong.

Our results confirm the strong sensitivity of temperatures to ozone in the TTL [e.g., *McElroy et al.*, 1992; *Thuburn and Craig*, 2002] using strongly idealized RCE calculations with ad hoc changes in ozone. This sensitivity is quantified further in Figure 12 (right). Note that higher ozone transition heights correspond to lower TTL ozone amounts; i.e., negative sensitivity of T_{CP} with respect to ozone transition refers to a positive feedback between TTL ozone and temperature. Unlike for the sensitivity to changes in q_{str}, imposed upwelling strongly enhances this positive feedback. In contrast to the water vapor sensitivity, the effect of upwelling can here be interpreted as lofting the cold point closer into the region of exponential increase of ozone, where its radiative impact on temperature structure is stronger. A corollary is that a strengthened Brewer-Dobson circulation (enhanced upwelling) with climate change, as predicted by current climate models [e.g., *Butchart et al.*, 2010], will produce a stronger positive ozone-temperature feedback in the TTL. *Gettelman et al.* [2010] pointed out that even though lower stratospheric ozone amounts decrease due to a strengthened Brewer-Dobson circulation, both cold point-level ozone amount and cold point temperature generally increase in climate models, which supports this hypothesized stronger positive ozone-temperature feedback. Ozone-circulation feedbacks have been found to play an important modifying role in climate change response experiments [e.g., *Dietmüller et al.*, 2014; *Nowack et al.*, 2015].

Our experiment setup incorporated interactive ozone in a very crude and ad hoc fashion. More accurate calculations, even for the highly idealized single-column settings as considered here, require an interactive ozone chemistry scheme coupled to the radiative scheme and parameterizations for tropospheric (fast) and stratospheric (slow) transport. For example, transport due to upwelling modifies the ozone and water vapor distributions around the tropopause, which will then exert a feedback onto the temperature structure [e.g., *Fueglistaler et al.*, 2011]. The modified temperature structure then further alters the upwelling-induced dynamical cooling Q_{dyn}, because it is a function of the vertical temperature gradient. The correct simulation of these feedbacks may be crucial to narrow down the large spread in simulated cold point temperatures in climate models, which has in part been linked to TTL-level ozone variations in these models [*Gettelman et al.*, 2009]. Preliminary results based on RCE simulations with interactive ozone chemistry qualitatively confirm the strong sensitivity of the TTL temperature structure to ozone (not shown).

Our idealized setup allows us to perform a simple test to isolate the potential contribution due to ozone to the spread in cold point temperatures in chemistry-climate models (CCMs) — by prescribing ozone profiles based on the CCMs instead of the SHADOZ control profile. Note that all CCMs use interactive ozone chemistry (see appendix for details), unlike some of the climate models used for the climate model intercomparison projects [*Randel and Jensen*, 2013]. We impose a stratospheric upwelling acting on temperature of 0.5 mm/s as before. The resulting RCE temperature profiles using the CCM ozone profiles are shown as gray lines in Figure 13, compared to the control case using SHADOZ ozone (dashed lines in the figure). Details about the CCMs used are provided in the appendix.

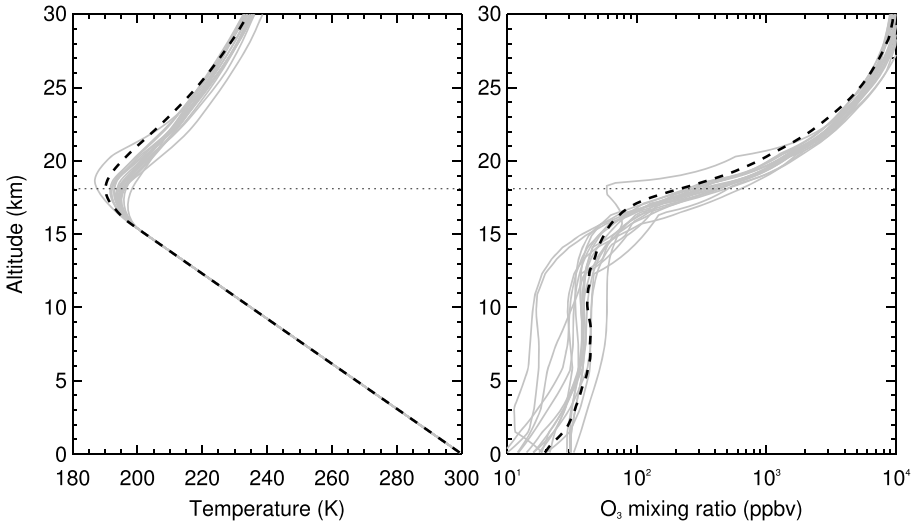

Figure 13. (left) RCE temperature profiles using (right) prescribed ozone profiles from the CCMs and imposed stratospheric upwelling of 0.5 mm/s. The dashed line on the left shows the reference RCE profile using the SHADOZ ozone climatology (shown as dashed line on the right). All solutions use prescribed stratospheric water vapor amount of 4 ppmv. All other settings are identical to those used for the other RCE solutions discussed in the paper.

Almost all CCMs exhibit a high bias in tropopause-level ozone compared to SHADOZ. One outlier CCM (CNRM-ACM) exhibits a strong low bias near the tropopause and in the lowermost stratosphere. Except for this outlier model, the high ozone bias near the tropopause causes higher RCE cold point temperatures than in the control case (by ~5 K on average). Excluding the outlier, the spread in simulated T_{CP} due to the ozone differences is about 6 K (including the outlier increases the spread to 10 K)—the same order of magnitude as the full spread in CCM cold point temperatures (see below). The differences in simulated ozone in CCMs alone can therefore cause substantial spread in their cold point temperatures, with corresponding consequences for simulated stratospheric water vapor content and its climate effects. Of course, other model differences cause further spread, e.g., different residual circulation strengths. An inspection of the associated spread in radiative heating rates reveals that both shortwave heating and longwave heating contribute, with a somewhat larger contribution due to longwave heating.

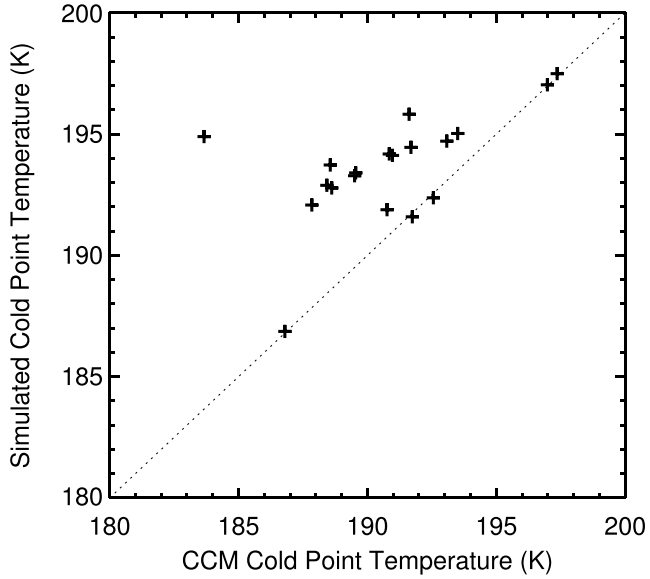

Figure 14. Simulated cold point temperatures in RCE with imposed uniform upwelling of 0.5 mm/s and using ozone profiles from the CCMs (corresponding to the RCE profiles shown in Figure 13) versus cold point temperatures from the models.

Figure 14 supports the suspicion that the ozone differences alone can explain a large fraction of the inter-model spread in T_{CP}: excluding the outlier model, our simulated T_{CP} is correlated with the CCM values at 0.76 (the correlation coefficient drops to 0.57 when including the outlier). Five of the CCMs fall almost exactly on the 1:1 line (dotted). We have tested whether using the vertically dependent upwelling from the individual CCMs improves this correlation and found, somewhat surprisingly, that it instead significantly reduces the correlation but leads to an overall larger spread (not shown). Our goal here is not to reproduce the CCM's T_{CP} values, but rather to demonstrate the strong radiative effects due to ozone, so we have not pursued the issue of model spread further.

In closing we note that the sensitivities explored in this paper also result in significant changes in the height and temperature of the convection top. Lower stratospheric water vapor concentrations and lower TTL ozone concentrations lead to a cooling by several kelvins and lofting by up to 1 km of the convection top. In principle, one would expect anvil clouds and detrainment to peak around the convection top. Our calculations then suggest that the environmental variables considered here are able to modify anvil temperatures, in contrast to the fixed-anvil-temperature hypothesis in its initial form [*Hartmann and Larson*, 2002] but broadly consistent with the cloud-resolving model results of *Kuang and Hartmann* [2007] and *Harrop and Hartmann* [2012]. Our results also suggest that stratospheric tropical upwelling leads to cooling and lofting of the convection top. However, the calculations did not include the effect of upper tropospheric lapse rate adjustments and cloud-radiative effects, which could modify the changes in convection top temperature.

Appendix A

For the results shown in Figures 13 and 14 we use CCM output from the Chemistry Climate Model Validation (CCMVal-2) activity within SPARC (Stratosphere-troposphere Processes And their Role in Climate) [*SPARC CCMVal*, 2010]. The CCMs used are (in alphabetical order) as follows: AMTRAC3, CAM3.5, CCSRNIES, CMAM, CNRM-ACM, E39CA, EMAC, EMAC-FUB, GEOSCCM, LMDZrepro, MRI, Niwa_SOCOL, SOCOL, ULAQ, UMETRAC, UMSLIMCAT, UMUKCA-METO, UMUKCA-UCAM, and WACCM. All CCMs provide ozone data in the region of interest (TTL and lowermost stratosphere). Some have missing data either below this region or higher up in the stratosphere, i.e., in regions that hardly affect TTL temperatures. To still include these CCMs in our analysis, we filled the missing data in these CCMs with data from another CCM with the same underlying model core: UMETRAC data have been used at and below 200 hPa and above 0.5 hPa for missing UMSLIMCAT data, WACCM data have been used above the model top of 5 hPa for CAM3.5, and EMAC data have been used above the model top of 10 hPa for E39CA. The ozone profiles shown in Figure 13 correspond to the January 1979–2005 climatology at 10°S from the historical (REF-B1) runs, which use observed forcings and sea surface temperatures (except for CMAM, which was the only model with a coupled ocean).

Acknowledgments

This work was supported by a CAREER grant of the U.S. National Science Foundation's Climate and Large-Scale Dynamics Program under grant 1151768. ERA-Interim data were provided by ECMWF through NCAR (ERA-I data can be found at http://apps.ecmwf.int/datasets/data/interim-full-daily/levtype=ml/). We thank Sasha Glanville for help with the MLS data used in Figure 1 (MLS data can be found at http://disc.gsfc.nasa.gov/datacollection/ML2H2O_003.html). Helpful comments during the course of this work were provided by John Albers and Peter Hitchcock. We are grateful to Kenneth Minschwaner for pointing out the *McElroy et al.* [1992] reference, which we had not been aware of until after this work was completed. Two anonymous reviewers are thanked for their detailed comments which greatly helped to improve the clarity of the presentation.

References

Abalos, M., F. Ploeger, P. Konopka, W. J. Randel, and E. Serrano (2013), Ozone seasonality above the tropical tropopause: Reconciling the Eulerian and Lagrangian perspectives of transport processes, *Atmos. Chem. Phys.*, *13*, 10,787–10,794, doi:10.5194/acp-13-10787-2013.

Abalos, M., B. Legras, F. Ploeger, and W. J. Randel (2015), Evaluating the advective Brewer-Dobson circulation in three reanalyses for the period 1979–2012, *J. Geophys. Res. Atmos.*, *120*, 7534–7554, doi:10.1002/2015JD023182.

Avallone, L. M., and M. J. Prather (1996), Photochemical evolution of ozone in the lower tropical stratosphere, *J. Geophys. Res.*, *101*, 1457–1461.

Birner, T. (2010), Residual circulation and tropopause structure, *J. Atmos. Sci.*, *67*, 2582–2600.

Brewer, A. W. (1949), Evidence for a world circulation provided by the measurements of helium and water vapor distribution in the stratosphere, *Q. J. R. Meteorol. Soc.*, *75*, 351–363.

Butchart, N., et al. (2010), Chemistry-climate model simulations of 21st century stratospheric climate and circulation changes, *J. Clim.*, *23*, 5349–5374.

Chae, J. H., and S. C. Sherwood (2007), Annual temperature cycle of the tropical tropopause: A simple model study, *J. Geophys. Res.*, *112*, D19111, doi:10.1029/2006JD007956.

Dee, D. P., et al. (2011), The ERA-Interim reanalysis: Configuration and performance of the data assimilation system, *Q. J. R. Meteorol. Soc.*, *137*, 553–597, doi:10.1002/qj.828.

Dietmüller, S., M. Ponater, and R. Sausen (2014), Interactive ozone induces a negative feedback in CO_2-driven climate change simulations, *J. Geophys. Res. Atmos.*, *119*, 1796–1805, doi:10.1002/2013JD020575.

Fels, S. B., J. D. Mahlman, M. D. Schwarzkopf, and R. W. Sinclair (1980), Stratospheric sensitivity to perturbations in ozone and carbon dioxide: Radiative and dynamical response, *J. Atmos. Sci.*, *37*, 2265–2297.

Folkins, I., M. Loewenstein, J. Podolske, S. J. Oltmans, and M. Proffitt (1999), A barrier to vertical mixing at 14 km in the tropics: Evidence from ozonesondes and aircraft measurements, *J. Geophys. Res.*, *D18*, 22,095–22,102.

Folkins, I., C. Braun, A. M. Thompson, and J. White (2002), Tropical ozone as indicator of deep convection, *J. Geophys. Res.*, *107*(D13), 4184, doi:10.1029/2001JD001178.

Forster, P. M., G. Bodeker, R. Schofield, S. Solomon, and D. Thompson (2007), Effects of ozone cooling in the tropical lower stratosphere and upper troposphere, *Geophys. Res. Lett.*, *34*, L23813, doi:10.1029/2007GL031994.

Forster, P. M. d. F., and K. P. Shine (1999), Stratospheric water vapour changes as a possible contributor to observed stratospheric cooling, *Geophys. Res. Lett.*, *26*, 3309–3312.

Fueglistaler, S., A. E. Dessler, T. J. Dunkerton, I. Folkins, Q. Fu, and P. W. Mote (2009), Tropical tropopause layer, *Rev. Geophys.*, *47*, RG1004, doi:10.1029/2008RG000267.

Fueglistaler, S., P. H. Haynes, and P. M. Foster (2011), The annual cycle in lower stratospheric temperatures revisited, *Atmos. Chem. Phys.*, *11*, 3701–3711, doi:10.5194/acp-11-3701-2011.

Gettelman, A., and T. Birner (2007), Insights into tropical tropopause layer processes using global models, *J. Geophys. Res.*, *112*, D23104, doi:10.1029/2007JD008945.

Gettelman, A., P. M. de F. Forster, M. Fujiwara, Q. Fu, H. Vömel, L. K. Gohar, C. Johanson, and M. Ammerman (2004), Radiation balance of the tropical tropopause layer, *J. Geophys. Res.*, *109*, D07103, doi:10.1029/2003JD004190.

Gettelman, A., et al. (2009), The tropical tropopause layer 1960–2100, *Atmos. Chem. Phys.*, *9*, 1621–1637.

Gettelman, A., et al. (2010), Multi-model assessment of the upper troposphere and lower stratosphere: Tropics and global trends, *J. Geophys. Res.*, *115*, D00M08, doi:10.1029/2009JD013638.
Gilford, D. M., and S. Solomon (2017), Radiative effects of stratospheric seasonal cycles in the tropical upper troposphere and lower stratosphere, *J. Clim.*, *30*, 2769–2783, doi:10.1175/JCLI-D-16-0633.1.
Glanville, A. A., and T. Birner (2017), Role of vertical and horizontal mixing in the tape recorder signal near the tropical tropopause, *Atmos. Chem. Phys.*, *17*, 4337–4353, doi:10.5194/acp-17-4337-2017.
Harrop, B. E., and D. L. Hartmann (2012), Testing the role of radiation in determining tropical cloud-top temperature, *J. Clim.*, *25*, 5731–5747, doi:10.1175/JCLI-D-11-00445.1.
Hartmann, D. L., and K. Larson (2002), An important constraint on tropical cloud-climate feedback, *Geophys. Res. Lett.*, *29*(20), 1951, doi:10.1029/2002GL015835.
Highwood, E. J., and B. J. Hoskins (1998), The tropical tropopause, *Q. J. R. Meteorol. Soc.*, *124*, 1579–1604.
Hitchcock, P., T. G. Shepherd, and S. Yoden (2010), On the approximation of local and linear radiative damping in the middle atmosphere, *J. Atmos. Sci.*, *67*, 2070–2085, doi:10.1175/2009JAS3286.1.
Holton, J. R., P. H. Haynes, M. E. McIntyre, A. R. Douglas, R. B. Rood, and L. Pfister (1995), Stratosphere-troposphere exchange, *Rev. Geophys.*, *33*, 403–439.
Kim, J., K. M. Grise, and S.-W. Son (2013), Thermal characteristics of the cold-point tropopause region in CMIP5 models, *J. Geophys. Res. Atmos.*, *118*, 8827–8841, doi:10.1002/jgrd.50649.
Konopka, P., et al. (2007), Contribution of mixing to upward transport across the Tropical Tropopause Layer (TTL), *Atmos. Chem. Phys.*, *7*, 3285–3308.
Kuang, Z., and D. L. Hartmann (2007), Testing the fixed anvil temperature hypothesis in a cloud-resolving model, *J. Clim.*, *20*, 2051–2057, doi:10.1175/JCLI4124.1.
Livesey, N. J., et al. (2007), EOS MLS version 2.2 Level 2 data quality and description document, Tech. Rep. JPL D-33509, Jet Propul. Lab., Pasadena, Calif.
Manabe, S., and B. G. Hunt (1968), Experiments with a stratospheric general circulation model: I. Radiative and dynamic aspects, *Mon. Weather Rev.*, *96*(8), 471–502, doi:10.1175/1520-0493(1968)096<0477:EWASGC>2.0.CO;2.
Manabe, S., and R. F. Strickler (1964), Thermal equilibrium of the atmosphere with a convective adjustment, *J. Atmos. Sci.*, *21*, 361–385.
Maycock, A. C., M. M. Joshi, K. P. Shine, and A. A. Scaife (2013), The circulation response to idealized changes in stratospheric water vapor, *J. Clim.*, *26*, 545–561, doi:10.1175/JCLI-D-12-00155.1.
McElroy, M. B., R. J. Salawitch, and K. Minschwaner (1992), The changing stratosphere, *Planet. Space Sci.*, *40*, 373–401.
Ming, A., A. C. Maycock, P. Hitchcock, and P. Haynes (2017), The radiative role of ozone and water vapour in the annual temperature cycle in the tropical tropopause layer, *Atmos. Chem. Phys.*, *17*, 5677–5701, doi:10.5194/acp-17-5677-2017.
Mlawer, E. J., S. Taubman, P. Brown, M. Iacono, and S. Clough (1997), RRTM, a validated correlated-k model for the longwave, *J. Geophys. Res.*, *102*, 16,663–16,682.
Mote, P. W., K. H. Rosenlof, M. E. McIntyre, E. S. Carr, J. C. Gille, J. R. Holton, J. S. Kinnersley, H. C. Pumphrey, J. M. R. III, and J. W. Waters (1996), An atmospheric tape recorder: The imprint of tropical tropopause temperatures on stratospheric water vapor, *J. Geophys. Res.*, *101*, 3989–4006, doi:10.1029/95JD03422.
Nowack, P. J., N. Luke Abraham, A. C. Maycock, P. Braesicke, J. M. Gregory, M. M. Joshi, A. Osprey, and J. A. Pyle (2015), A large ozone-circulation feedback and its implications for global warming assessments, *Nat. Clim. Change*, *5*(1), 41–45, doi:10.1038/nclimate2451.
Paulik, L. C., and T. Birner (2012), Quantifying the deep convective temperature signal within the Tropical Tropopause Layer (TTL), *Atmos. Chem. Phys.*, *12*, 12,183–12,195.
Ploeger, F., P. Konopka, R. Müller, S. Fueglistaler, T. Schmidt, J. C. Manners, J. U. Grooß, G. Günther, P. M. Forster, and M. Riese (2012), Horizontal transport affecting trace gas seasonality in the tropical tropopause layer (TTL), *J. Geophys. Res.*, *117*, D09303, doi:10.1029/2011JD017267.
Randel, W. J., and E. J. Jensen (2013), Physical processes in the tropical tropopause layer and their roles in a changing climate, *Nat. Geosci.*, *6*, 169–176, doi:10.1038/ngeo1733.
Randel, W. J., R. R. Garcia, and F. Wu (2002), Time-dependent upwelling in the tropical lower stratosphere estimated from the zonal-mean momentum budget, *J. Atmos. Sci.*, *59*, 2141–2152.
Randel, W. J., F. Wu, and P. Forster (2007a), The extratropical tropopause inversion layer: Global observations with GPS data, and a radiative forcing mechanism, *J. Atmos. Sci.*, *64*, 4489–4496.
Randel, W. J., M. Park, F. Wu, and N. Livesey (2007b), A large annual cycle in ozone above the tropical tropopause linked to the Brewer-Dobson Circulation, *J. Atmos. Sci.*, *64*(12), 4479–4488, doi:10.1175/2007JAS2409.1.
Solomon, S., K. H. Rosenlof, R. W. Portman, J. S. Daniel, S. M. Davies, T. J. Sanford, and G.-K. Plattner (2010), Contributions of stratospheric water vapor to decadal changes in the rate of global warming, *Science*, *327*, 1219–1223.
SPARC CCMVal (2010), SPARC Report on the Evaluation of Chemistry- Climate Models, edited by V. Eyring, T. G. Shepherd, and D. W. Waugh, SPARC Report No. 5, WCRP-132, WMO/TD-No. 1526. [Available at http://www. atmosp.physics.utoronto.ca/SPARC.]
Thompson, A. M., et al. (2003), Southern Hemisphere Additional Ozonesondes (SHADOZ) 1998–2000 tropical ozone climatology: 1. Comparison with Total Ozone Mapping Spectrometer (TOMS) and ground-based measurements, *J. Geophys. Res.*, *108*, 8238, doi:10.1029/2001JD000967.
Thuburn, J., and G. C. Craig (2002), On the temperature structure of the tropical substratosphere, *J. Geophys. Res.*, *107*(D2), 4017, doi:10.1029/2001JD000448.
Yang, Q., Q. Fu, and Y. Hu (2010), Radiative impacts of clouds in the tropical tropopause layer, *J. Geophys. Res.*, *115*, D00H12, doi:10.1029/2009JD012393.